NASA/TM-2006-213675

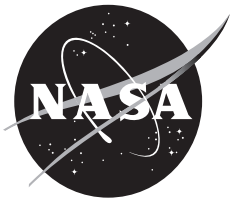

Photogrammetric Trajectory Estimation of Foam Debris Ejected From an F-15 Aircraft

Mark S. Smith
NASA Dryden Flight Research Center
Edwards, California

April 2006

NASA STI Program ... in Profile

Since its founding, NASA has been dedicated to the advancement of aeronautics and space science. The NASA scientific and technical information (STI) program plays a key part in helping NASA maintain this important role.

The NASA STI program is operated under the auspices of the Agency Chief Information Officer. It collects, organizes, provides for archiving, and disseminates NASA's STI. The NASA STI program provides access to the NASA Aeronautics and Space Database and its public interface, the NASA Technical Report Server, thus providing one of the largest collections of aeronautical and space science STI in the world. Results are published in both non-NASA channels and by NASA in the NASA STI Report Series, which includes the following report types:

- TECHNICAL PUBLICATION. Reports of completed research or a major significant phase of research that present the results of NASA programs and include extensive data or theoretical analysis. Includes compilations of significant scientific and technical data and information deemed to be of continuing reference value. NASA counterpart of peer-reviewed formal professional papers but has less stringent limitations on manuscript length and extent of graphic presentations.

- TECHNICAL MEMORANDUM. Scientific and technical findings that are preliminary or of specialized interest, e.g., quick release reports, working papers, and bibliographies that contain minimal annotation. Does not contain extensive analysis.

- CONTRACTOR REPORT. Scientific and technical findings by NASA-sponsored contractors and grantees.

- CONFERENCE PUBLICATION. Collected papers from scientific and technical conferences, symposia, seminars, or other meetings sponsored or cosponsored by NASA.

- SPECIAL PUBLICATION. Scientific, technical, or historical information from NASA programs, projects, and missions, often concerned with subjects having substantial public interest.

- TECHNICAL TRANSLATION. English-language translations of foreign scientific and technical material pertinent to NASA's mission.

Specialized services also include creating custom thesauri, building customized databases, and organizing and publishing research results.

For more information about the NASA STI program, see the following:

Access the NASA STI program home page at *http://www.sti.nasa.gov*.

- E-mail your question via the Internet to help@sti.nasa.gov.

- Fax your question to the NASA STI Help Desk at (301) 621-0134.

- Phone the NASA STI Help Desk at (301) 621-0390.

- Write to:
  NASA STI Help Desk
  NASA Center for AeroSpace Information
  7121 Standard Drive
  Hanover, MD 21076-1320

NASA/TM-2006-213675

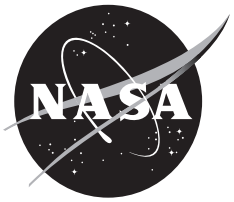

Photogrammetric Trajectory Estimation of Foam Debris Ejected From an F-15 Aircraft

Mark S. Smith
NASA Dryden Flight Research Center
Edwards, California

National Aeronautics and
Space Administration

Dryden Flight Research Center
Edwards, California 93523-0273

April 2006

NOTICE

Use of trade names or names of manufacturers in this document does not constitute an official endorsement of such products or manufacturers, either expressed or implied, by the National Aeronautics and Space Administration.

Available from the following:

NASA Center for AeroSpace Information
7121 Standard Drive
Hanover, MD 21076-1320
(301) 621-0390

National Technical Information Service
5285 Port Royal Road
Springfield, VA 22161-2171
(703) 605-6000

ABSTRACT

Photogrammetric analysis of high-speed digital video data was performed to estimate trajectories of foam debris ejected from an F-15B aircraft. This work was part of a flight test effort to study the transport properties of insulating foam shed by the Space Shuttle external tank during ascent. The conical frustum-shaped pieces of debris, called "divots," were ejected from a flight test fixture mounted underneath the F-15B aircraft. Two onboard cameras gathered digital video data at two thousand frames per second. Time histories of divot positions were determined from the videos post flight using standard photogrammetry techniques. Divot velocities were estimated by differentiating these positions with respect to time. Time histories of divot rotations were estimated using four points on the divot face. Estimated divot position, rotation, and Mach number for selected cases are presented. Uncertainty in the results is discussed.

NOMENCLATURE

A	least-squares regressor matrix (m x p)
AFTF	Aerodynamic Flight Test Fixture
B	dependent variables in least-squares model (m x 1)
d	divot axis direction vector (3 x 1)
DLT	direct linear transformation
g	matrix component of divot axes unit vector
G	matrix of divot axes unit vectors
L	direct linear transformation equation coefficient
m	number of elements in **B** vector
P	point location vector (3 x 1)
p	number of unknown parameters in least-squares model
X, Y	location of point on image, pixels
x, y, z	location of point in space, ft
ξ	least-squares vector of unknown parameters (p x 1)
σ	estimated standard error of unknown parameter
ϕ	rotation angle about x-axis, deg
Γ	Euler angle rotation matrix (3 x 3)

θ	rotation angle about y-axis, deg
ν	error components in least-squares model
ψ	rotation angle about z-axis, deg

superscripts

T	transpose
-1	matrix inverse

INTRODUCTION

A series of flight tests was conducted to evaluate the structural survivability of Space Shuttle external tank insulating foam debris in a real flight environment (ref. 1). These tests were part of an effort by NASA to understand the behavior of foam pieces, or "divots," shed by the external tank during ascent. To simulate this phenomenon, divots were ejected from a test fixture mounted underneath an F-15B aircraft. Ejections were performed at flight conditions relevant to the ascent trajectory of the Space Shuttle.

The products of these tests were high-speed digital videos of divot ejections, recorded onboard the aircraft. The primary data reduction technique was qualitative analysis of these videos. Of key interest was whether the divots broke up or stayed intact at various flight conditions. Also of interest were the aerodynamic characteristics of the divots. The videos showed whether the divots tumbled or they trimmed to a stable orientation and flew.

A supplemental means of analyzing video was quantification of divot trajectories through the use of photogrammetry – "the process of deriving (usually) metric information about an object through measurements made on photographs of the object (ref. 2)." Using geometric principles, the location of a point in space can be triangulated using its position in multiple images. Photogrammetry has many uses in a wide variety of fields from biomechanics to surveying and has been used in wind tunnel tests to measure model deformation (ref. 3). In-flight photogrammetry has previously been used to evaluate store separation (ref. 4). For this project, frame-by-frame estimates of divot position and orientation were desired.

This paper discusses the technique used to estimate divot trajectories. A method for estimating divot orientation angles using multiple points on the divots is also presented. Uncertainty in the results is discussed, and selected results from two flight conditions are shown.

TEST SETUP

Figure 1 shows the test aircraft, an F-15B built by McDonnell Aircraft Company (now Boeing, St. Louis, MO). This aircraft has been modified in several ways to serve as a research test bed. One substantial modification is the addition of a vertical fin mounted at the centerline on the lower fuselage (ref. 5). This fin, known as the Aerodynamic Flight Test Fixture (AFTF), can be used for

various kinds of aerodynamic research. Figure 2 shows a diagram of the AFTF. The basic length of the fixture is 107.0 inches, but an ogive tail was added to reduce drag. The AFTF is 8.0 inches wide, 32.0 inches tall, and features several bays for instrumentation, accessible via removable side panels.

For this series of tests, the AFTF was equipped with foam sheets consisting of aluminum plates sprayed with two-inch thick external tank foam (ref. 1). Cylindrical voids were cut into the backs of the foam sheets, next to the aluminum, to simulate the air pockets that may cause divots to be shed from the external tank of the Shuttle. Figure 3 illustrates the divots and some of the terminology relating to them. A pneumatic system inside the AFTF was used to eject divots by releasing high-pressure nitrogen gas into the voids. The flight crew triggered this system from the cockpit. Resulting divot sizes varied depending on the void size. Void diameters varied from 0.31 to 1.68 inches and resulting divot diameters ranged from approximately 1.5 to 5.5 inches (ref. 1). The divots were given letter designations, "A" through "I," based on their location, as shown in figure 2.

The aircraft was equipped with two flight-qualified, high-speed digital video cameras, housed in pods mounted to the fore and aft missile rails (ref. 1) (fig. 4). For some flights, only one camera was operational. Each pod was equipped with a removable one-quarter-inch thick viewing window made of borosilicate crown optical glass. Figure 5 shows the position of the pods relative to the AFTF and the camera viewing angles (ref. 1). The forward pod was 46 inches long; the aft pod was 50.8 inches long. Both pods were 8 inches deep. These pods were designed to impact the local airflow as little as possible. For instance, inboard surfaces were designed to be parallel to the freestream flow to avoid creating shocks that would impinge on the AFTF. The cameras were oriented to capture approximately 5 feet of divot travel downstream from the ejection point. The field of view for the forward camera was roughly 34 degrees; the field of view for the aft camera was roughly 67 degrees. Aiming and focusing of the cameras were performed on the ground prior to the flights. The only camera motion relative to the AFTF during the tests was a result of structural deformation and vibration.

The cameras recorded images at 2 000 frames per second (500 microseconds per frame) with an exposure time of 50 microseconds. A synchronization system was designed to link the cameras together to the divot ejection system and the cockpit controls (ref. 1). The exposure of each camera was synchronized to one microsecond. Each ejection trigger from the cockpit would tell the cameras to record for a brief time. The resulting color videos, 1 280 by 512 pixels per frame, were downloaded to a laptop computer following each flight. Composite images from both cameras of an E-divot ejection are shown in figures 6 and 7. No frames were skipped in the making of these figures. Figure 8 is a postflight image of two of the foam sheets, from which divots A through C and G through I were ejected.

As mentioned previously, flight conditions were designed to match points along the Shuttle ascent trajectory. The maximum Mach number test point was at approximately Mach 2.0 and at an altitude of 48 354 feet. The maximum dynamic pressure test point was at approximately Mach 1.6 at an altitude of 36 124 feet, which corresponds to a dynamic pressure

of 848 lbf/ft^2. Divots were also ejected at subsonic conditions. A total of 41 successful divot ejections occurred. Of these, only 13 occurred with both cameras operational.

METHODS OF ANALYSIS

This section describes the techniques used for the photogrammetric analysis. An attempt was made to estimate divot position and orientation with data from only one camera, because a large number of ejections took place with only one camera operational. A technique capitalizing on the physical relationship between multiple points on each divot was used (ref. 7). While this worked with test objects, the technique was too sensitive for practical use with divots because there were no reference points with locations that were known precisely enough. As such, only the two-camera photogrammetry methodology is presented. The procedure used to calibrate the cameras is discussed and the mathematical concept of *direct linear transformation* (DLT) is presented. The divot tracking procedure is described. A method for estimating divot orientation is also described.

Direct Linear Transformation

The standard approach to doing photogrammetry is based on the assumption that points in space are connected to their images by straight lines through the perspective center of the camera, a principle called *collinearity* (ref. 3). The mathematical formulation of the problem can be reduced to the following equations:

$$X + \frac{L_1 x + L_2 y + L_3 z + L_4}{L_9 x + L_{10} y + L_{11} z + 1} = 0 \tag{1}$$

$$Y + \frac{L_5 x + L_6 y + L_7 z + L_8}{L_9 x + L_{10} y + L_{11} z + 1} = 0 \tag{2}$$

These are known as the DLT form of the collinearity equations (ref. 3). In these equations, $\{x, y, z\}$ is a point location in space and $\{X, Y\}$ is its location in the image, in pixels. The origin of the image coordinate system is located at the upper left-hand corner of the image, with X increasing to the right and Y increasing down.

The intrinsic parameters of the camera, such as focal length and principal point, do not need to be explicitly calculated because they are contained in the L coefficients. The L coefficients also include information about the position and orientation of the camera. Equations (1) and (2) contain no compensation for lens distortion. It is possible to account for radial, asymmetric, and affine distortion by adding additional terms, depending on the desired model (ref. 7). Addition of new terms substantially increases the complexity of the problem by adding nonlinearity to the parameters.

One set of L coefficients must be determined for each camera and can be estimated using a least-squares fit to calibration data. Each point on the image provides two equations, according to eqs. (1) and (2). These equations can be rearranged into functions of the L coefficients and arranged into a system of equations:

$$\begin{bmatrix} X_1 \\ Y_1 \\ \vdots \\ X_n \\ Y_n \end{bmatrix} = - \begin{bmatrix} x_1 & y_1 & z_1 & 1 & 0 & 0 & 0 & 0 & X_1x_1 & X_1y_1 & X_1z_1 \\ 0 & 0 & 0 & 0 & x_1 & y_1 & z_1 & 1 & Y_1x_1 & Y_1y_1 & Y_1z_1 \\ \vdots & \vdots & \vdots & \vdots & \vdots & \vdots & \vdots & \vdots & \vdots & \vdots & \vdots \\ x_n & y_n & z_n & 1 & 0 & 0 & 0 & 0 & X_nx_n & X_ny_n & X_nz_n \\ 0 & 0 & 0 & 0 & x_n & y_n & z_n & 1 & Y_nx_n & Y_ny_n & Y_nz_n \end{bmatrix} \begin{bmatrix} L_1 & \cdots & L_{11} \end{bmatrix}^T \quad (3)$$

where n is the total number of calibration points. As there are eleven unknowns, at least six calibration points with known coordinates are required to make an over determined system. The least-squares problem for the system in eq. (3) is of the form (ref. 8):

$$\mathbf{B} = \mathbf{A}\xi + v \quad (4)$$

where v represents error components. The estimated value of ξ, the matrix of L coefficients, that corresponds to the minimum square error between the measured **B** vector and the model output is

$$\hat{\xi} = \left[\mathbf{A}^T \mathbf{A} \right]^{-1} \mathbf{A}^T \mathbf{B} \quad (5)$$

The estimated parameter covariance matrix is calculated using the equations:

$$Cov\left(\hat{\xi}\right) = \hat{\sigma}^2 \left(\mathbf{A}^T \mathbf{A} \right)^{-1} \quad (6)$$

$$\hat{\sigma}^2 = \frac{\left(\mathbf{B} - \mathbf{A}\xi\right)^T \left(\mathbf{B} - \mathbf{A}\xi\right)}{m - p} \quad (7)$$

where m is the number of elements in the **B** vector and p is the number of unknown parameters (11 in this case). Standard errors of the estimated parameters are the square roots of the diagonal terms in the covariance matrix.

One traditional way of defining the calibration points is by measuring them using a theodolite. The pace of the project and the secondary priority of the photogrammetric analysis did not allow for such measurements, however. For this study, calibration was performed using a test bracket with a large metal plate that was one-eighth of an inch thick. Checkerboard patterns with two-inch

squares were affixed to both sides of the plate. The checkerboard patterns were used to suit a camera calibration software tool that was, in the end, not used for this study (ref. 9). The bracket rested on top of the AFTF and was placed so that the patterns were perpendicular to the surface, as shown in figure 9. The bracket was aligned with the trailing edge of each vertical reference stripe. The reference coordinate system chosen for the trajectory analysis is also shown in figure 9. For simplicity, the axes were aligned with conventional aircraft axes – the x-axis extending out the aircraft nose, the y-axis out the right wing, and the z-axis downward. The origin was chosen to be on the AFTF surface at the stripe immediately forward of the foam sheet from which the D through F divots were ejected. The z-axis location of the origin was the bottom edge of the checkerboard.

Reference photos were taken with the checkerboard pattern at the seven reference stripes that were spaced at one-foot intervals along the AFTF. For practical purposes, only images at five stations were useable by the front camera and only six by the rear camera. The pixel coordinates of the corners of the two-inch squares were located by means of a corner-finding algorithm (ref. 9) and these coordinates were used as reference points. Unfortunately, the bottom of the checkerboard pattern was at roughly the same height as the ejection locations of the A through F divots. This would mean that if those divots traveled downward they would be out of the calibrated volume. (Note that this would not have affected calibrations using the technique of ref. 9.) With this problem in mind, other known locations, such as the bottoms of the reference stripes and corners of the calibration fixture, were used to expand the calibration volume 7 inches downward. These coordinates were combined with the checkerboard points to form one data set that was used to estimate the 11 DLT coefficients for each camera. As a consequence, considerably more than the minimum number of calibration points was used: 209 for the front camera and 548 for the aft. The discrepancy in the number of calibration points was a result of the limited view of the calibration fixture from the front camera.

Spatial positions of targets $\{x, y, z\}$ can then be estimated (or *triangulated*) using multiple camera images, eqs. (1) and (2), and the estimated L coefficients. The set of equations from each camera represents a line in space on which the target lies. Ideally, lines from multiple cameras would intersect at the true location of the target. In practice, however, the lines do not quite meet and the target location that best fits them must be estimated. To do this, the DLT equations are rearranged so that $\{x, y, z\}$ are the unknowns:

$$\left(L_1 + XL_9\right)x + \left(L_2 + XL_{10}\right)y + \left(L_3 + XL_{11}\right)z = -\left(X + L_4\right) \tag{8}$$

$$\left(L_5 + YL_9\right)x + \left(L_6 + YL_{10}\right)y + \left(L_7 + YL_{11}\right)z = -\left(Y + L_8\right) \tag{9}$$

There will be one set of eqs. (8) and (9) for each camera, creating a system of four equations and three unknowns. Target locations $\{X, Y\}$ in pixel coordinates are gathered from the images and used in the equations. The method of least-squares is then used to solve the system as described previously.

Divot Tracking

To estimate the trajectory of a divot, its position in the videos had to be tracked to produce the {*X*, *Y*} pixel values used by the triangulation techniques. A commercial software package was used to process the video data (ref. 10). Given the relatively small number of applicable video frames for each case (roughly 20 for each camera), manual tracking was suitable. A crosshair was placed on the desired pixel in each frame. The software made it convenient to move back and forth temporally through the videos and to zoom in and out as necessary to track points. Also, brightness and contrast of the videos could be adjusted to enhance the view of the divots. Given the suboptimal lighting conditions, and the viewing angle, divots were not always clear in the rear camera images for the first few frames following ejection. As such, the capabilities of the video software were very helpful. The video software also made it possible to switch between camera views during tracking, which was beneficial for matching target points.

During the initial frames, patterns on the divot face were visible by both cameras. For the trajectory estimation, the target point was the cross point, roughly in the middle of the larger face of the divot. The divots typically rotated, so that after four or five frames the patterns were no longer visible by the front camera. From there on, an attempt was made to track the spot in the forward camera video where the target would be, using the aft camera images as guides. Though clearly not ideal, the difference in targets was deemed acceptable for this project.

The same analyst processed all divot trajectories for which videos from both cameras were available. A script was created to export frame numbers and corresponding {*X*, *Y*} positions to a text file. By retaining the frame numbers, the trajectory results could be easily correlated with the time stamps on the videos. The data from the text files were then used elsewhere for the triangulation and further analysis.

Estimation of Divot Orientation

Divot orientation was estimated by tracking four targets, $\mathbf{P}_1$ through $\mathbf{P}_4$, along the edge of each divot, as shown in figure 10. This figure also shows the axes system for the divot, with the x-axis emanating from the smaller face of the divot. From the illustration, it can be deduced that before ejection the divots are considered to be rotated 90° about the z-axis. At zero rotation ($\phi = \theta = \psi = 0°$), the divot axes system is aligned with the reference axes system defined previously (fig. 9). Tracking was performed in the same manner as previously described. The edge of the heavy vertical stripe was used as a guide for targets $\mathbf{P}_1$ and $\mathbf{P}_2$. The other two points chosen were perpendicular, based on visual inspection.

Again, after the first four or five frames, the divots rotated so that the patterns were not visible by the front camera and it was necessary to again approximate the targets based on their locations in the aft camera images. Tracking conditions were improved in this case, however, because the target points were not separated by the major thickness of the divot. Imperfections in the divot edge, such as notches, were used as guides. This technique was particularly helpful for gauging the rotation about the x-axis. The dominant rotation (about the z-axis) was easier to discern.

The $\{x, y, z\}$ coordinates of the four targets in the reference axes system were estimated as previously described. From those, vectors defining the directions of the y- and z-axes for each divot were computed:

$$\mathbf{d_y} = \mathbf{P_4} - \mathbf{P_3} \tag{10}$$

$$\mathbf{d_z} = \mathbf{P_2} - \mathbf{P_1} \tag{11}$$

The cross product of the two vectors yields a perpendicular one, i.e., a vector in the direction of the x axis:

$$\mathbf{d_x} = \mathbf{d_y} \times \mathbf{d_z} \tag{12}$$

The three directional vectors were normalized (thus creating unit vectors) and arranged into a matrix

$$\mathbf{G} = \begin{bmatrix} \dfrac{\mathbf{d_x}}{|\mathbf{d_x}|} & \dfrac{\mathbf{d_y}}{|\mathbf{d_y}|} & \dfrac{\mathbf{d_z}}{|\mathbf{d_z}|} \end{bmatrix} = \begin{bmatrix} g_{11} & g_{12} & g_{13} \\ g_{21} & g_{22} & g_{23} \\ g_{31} & g_{32} & g_{33} \end{bmatrix} \tag{13}$$

Recall that in divot axes, the x, y, and z unit vectors combine to form an identity matrix. As such, eq. (13) is equivalent to the rotation matrix that transfers those coordinates to the reference axes system (ref. 6). In terms of Euler angles for each divot (ϕ, θ, ψ), the rotation matrix is of the form (ref. 11):

$$\Gamma(\phi,\theta,\psi) = \begin{bmatrix} \cos\theta\cos\psi & \sin\phi\sin\theta\cos\psi - \cos\phi\sin\psi & \cos\phi\sin\theta\cos\psi + \sin\phi\sin\psi \\ \cos\theta\sin\psi & \sin\phi\sin\theta\sin\psi + \cos\phi\cos\psi & \cos\phi\sin\theta\sin\psi - \sin\phi\cos\psi \\ -\sin\theta & \sin\phi\cos\theta & \cos\phi\cos\theta \end{bmatrix} \tag{14}$$

If the **G** matrix represented an orthogonal system, it would be possible to calculate the Euler angles directly from the elements of Γ. Given the potential for errors in the position of the four target points, however, it is possible the estimated y- and z-axes were not orthogonal. No correction was done for this. A maximum-likelihood estimation technique was used to determine the set of Euler angles that made eq. (14) best match eq. (13). The resulting angles corresponded to an orthogonal set of axes. To reduce the number of iterations required by the solver, the estimated angles from the previous video frame were used as initial values.

RESULTS AND DISCUSSION

This section presents the results of the photogrammetry analysis, as well as comments on their accuracy. Results are shown for two flight conditions, Mach 1.2 at an altitude of 27,000 ft

and Mach 1.98 at an altitude of 47,000 ft. Three divots were tracked for each condition: D, E, and F. Divots D and F were approximately 5 inches in diameter; the E divots were roughly half that size (ref. 1).

Camera Calibration Results

Camera calibration using the previously described methodology went well. The least-squares fits to the calibration data were very good overall. Fit errors for the rear camera were mostly under 1 pixel in *X* and *Y*. All but 9 of the over 500 points had errors of less than 3 pixels. Residuals for the front camera were more scattered. In *Y*, the errors were typically under 2 pixels. Errors in *X* were larger in most cases, including a worst-case point that was off by nearly 9 pixels. The fit errors are a possible indication that distortion terms should be added to the DLT formulation for that camera.

To assess the stereo calibration of the system, the {x, y, z} locations were estimated for 72 calibration points that were shared between the two cameras. Although these points were used to estimate the DLT *L* coefficients, this can be considered a test of the triangulation capabilities of the two-camera model. A purer prediction test would have used points not used for calibration. Errors in the estimated locations were typically under 0.1 inches in each direction, though in the *x* direction they tended to be higher (roughly 0.2 inches in some cases). Taking into account the thickness of the calibration fixture, 0.125 inches, the errors in *x* are reasonable. The point with the biggest discrepancy had errors of 0.4 inches in the *x*, 0.5 inches in the *y*, and 0.25 inches in the *z* direction.

Accuracy Discussion

The researchers of reference 4 state the accuracy of their store separation trajectories as 0.5 inches in all axes. Reference 3 lists a position prediction accuracy of 0.02 inches, with extra uncertainties taking it out to 0.1 inches. In many respects, those cases were more ideal than this one. For instance, both studies used well-defined target points that were visible by all the cameras. The targets of ref. 3 were 3 to 5 pixels in diameter. For this project, the D and F divots started out at roughly 120 pixels in diameter in the front camera images. (The E divots were quite a bit smaller.) The orientation of the front camera leads to nearly a side view, so toward the end of the divot trajectories the divots took up approximately 50 pixels in *X* and 100 pixels in *Y*. In the rear camera images, divots were roughly 30 by 45 pixels at ejection and increased to about 80 by 60 pixels.

Camera motion during flights was small, 2 to 3 pixels at most, and was considered negligible for this analysis. The rear camera shifted noticeably, however, between ground and flight and even slightly (1 or 2 pixels) between flights. The shift in the rear camera view was approximately 3 pixels to the left and 18 pixels downward and can be seen by comparing figures 7 and 9. The front camera view shifted also, but only about 3 to 4 pixels. To determine the effect of these shifts, the bottoms of the vertical reference stripes of the AFTF were tracked and their {*x*, *y*, *z*} positions calculated. On average, the change in triangulated locations of the points was about 0.1 inches

in any direction, though a couple of points were changed by roughly 0.4 inches in both the x and the z. Some of the error may be attributed to tracking slightly different points. The least-squares generated standard errors for the in-flight positions (up to 0.95 inches) were considerably higher than those on the ground (nearly 0.01 inches). The discrepancy indicates increased mathematical confidence in the ground-based position estimates.

Another difference between ground and flight images, and another potential source of error, was lighting. Images on the ground were taken with an open shutter, as opposed to the 50-microsecond exposure time in flight. The very short exposure time resulted in poor lighting conditions and, as a result, the in-flight images were of lower quality. The decrease in quality often made the divot patterns, and in some cases the divots themselves, more difficult to discern. As a result, the potential for tracking errors was increased.

Given the large size of divots in the image and the inability to track a reference point with both cameras (in most cases), the ideal $\{X, Y\}$ location often times does not get chosen. Potential errors caused by this problem were investigated by offsetting the tracked points by a small amount in each direction and recomputing position. A nominal error of 3 pixels was used, which was scaled by a weighting factor to compensate for the relative size of the divot in the image. When the divot was largest in the frame (first frame for forward camera, last for the aft), the error was doubled because there was more potential for a bad choice. The weighting factor was equal to one when the divot was smallest in the frame, two when the divot was largest in frame, and changed linearly in between. Positions were calculated for the various combinations of offsets (9 for the front camera and 9 from the rear camera, for a total of 81 for each frame). The results were normally distributed with standard deviations of approximately 0.25 inches in each direction. The spread between the minimum and maximum values varied for each divot, but was typically on the order of an inch or less, and usually increased with x. The spread varies linearly with the nominal pixel error, so using a nominal error of 6 pixels would result in a range of approximately 2 inches.

For orientation estimates, ref. 4 states accuracies of 0.5º in pitch and yaw and 1º in roll. Again, that study utilized well-defined points visible to both cameras, as opposed to the setup encountered in this project. So, it can be assumed that those error values can be considered lower bounds (at best) of the uncertainties for this analysis. A method of assessing errors in divot orientation caused by tracking errors, similar to what was done for position, was attempted. However, the very large number of possible point combinations (3^{12}= 531 441) made it absurd. Spot uses of simplified versions of this technique estimated uncertainty values that were typically less than 10 degrees.

Since that technique did not work, orientation uncertainty was studied by retracking the four points used to define the axes of the divot and by recomputing the Euler angles, which essentially creates a set of different rotation "measurements." Since modifying the $\{X, Y\}$ pixel coordinates for one point suffices to change all the estimated orientation angles, a batch of several measurements was created without having to retrack all four control points each time. The same analyst performed the additional tracking. Figure 11 shows the results of this exercise for one D-divot ejection. The ranges between maximum and minimum values for θ and ψ were typically from 3° to 5º for this case. The smaller E divots were more sensitive to changes in tracking.

Trajectory Estimation Results

Trajectories were estimated for 10 divot ejections. Figures 12 and 13 show the estimated divot $\{x, y, z\}$ positions for ejections at two flight conditions. Mach number estimates are shown as well. Included in the plots are the least-squares-generated standard errors for the positions. Recall that the standard errors represent mathematical confidence in the results, and do not symbolize overall accuracy. No smoothing or curve fitting was performed on the trajectories. Divot velocities were calculated by first obtaining camera-relative divot speeds through numerically differentiating the trajectories, then subtracting those from the speed of the aircraft. Wind was neglected. Mach numbers were calculated using these velocities and local static temperature measurements from the AFTF instrumentation system.

The divots remained in the calibrated volume. Results indicate they only traveled approximately 1 foot laterally (y-axis) and less than ½ foot downward (z-axis) in the time shown. In that time, the divots traveled roughly 5 feet downrange from the ejection point, relative to the aircraft. Although technically the divots were in the calibrated space, the bulk of the calibration points were above where the divots traveled. Consequently, the results for these divots might be less accurate than they otherwise could be. Trajectories of the G, H, and I divots (recall figure 2) would likely not have suffered from this deficiency because they were ejected from spots well within the calibrated volume.

Orientation Estimation Results

Overall, the orientation estimation technique worked reasonably well, considering the difficulty in tracking the control points from the front camera. One item of interest is the skew angle between y- and z-axes of the divot calculated using eqs. (9) and (10), which is a measure of how well the initial problem was set up. Ideally, the angle should be 90º. Figure 14 shows an example of the variation of this angle not only by frame, but also with the retracking mentioned previously in the "Accuracy Discussion" section. Results shown are typical for the other divots; they were better in some cases and worse in others. The worst case was for one of the E divots, for which most of the tracking possibilities produced skew angles down to 50º. The orientation angle most affected by the skew was ϕ, the rotation angle about the axis of symmetry. The pitch of the divot, θ, was affected to a lesser extent and the rotation about the vertical axis, ψ, was fairly tolerant of changes.

Figures 15 and 16 show the median values of the divot Euler angle datasets generated by retracking the four control points as mentioned in the "Accuracy Discussion" section. The mean and median values of the sets were typically very similar. In cases where they disagreed, however, the median seemed to be the more appropriate of the two. As rotation about the z-axis was the dominant motion, the estimates of ψ have more confidence than ϕ and θ, which were smaller and more difficult to discern. While the patterns made this easier for the rear camera, they were typically out of the view of the front camera. The figures show that the estimated pre-ejection rotation angles were erroneous.

Trends were not very consistent for ϕ and θ, given the aforementioned discernment issues. Typically, ϕ remained within $\pm 25°$. The divot that exceeded this rotation, Divot F for the Mach 1.98 case, lost some of its edge shortly after ejection. As a result, it exhibited slightly different behavior than the others. For the Mach 1.2 flight condition, estimated θ, the tilt of the divots essentially stayed within ±15°. For the higher speed condition, two of the divots tilted forward roughly 40°.

Similar trends in ψ were seen for all the cases; however, the smaller divots rotated faster. From their starting point, the divots studied here always rotated initially so that their smaller side faced into the freestream flow. The divots were perpendicular to the airflow ($\psi = 0°$) within 0.003 seconds. They overshot this point by roughly 50° before reversing direction. In most cases, the divots would eventually stabilize to roughly $\psi = 0°$ beyond the region where they were visible by both cameras (i.e., where the photogrammetry analysis could not be performed).

CONCLUDING REMARKS

Photogrammetry was used to estimate trajectory information of conical frustum-shaped foam debris, or divots, ejected from an F-15B aircraft. This work was done to support a series of flight tests conducted for evaluating the structural survivability of Space Shuttle external tank insulating foam debris in a flight environment. The divots were ejected from a test fixture mounted underneath the aircraft and tracked using two high-speed digital cameras. Qualitative analysis of divot behavior from the videos was the primary intent of the flight test project.

The photogrammetry analysis was based on the concept of direct linear transformation (DLT). Camera calibration results were good for both cameras. Fit errors from calibration of the forward camera indicated that the addition of distortion terms to the DLT formulation might have been beneficial. Estimated trajectories were reasonable and showed that the divots stayed in the space covered by the camera calibration. The devised method of estimating orientation using four control points on the divot worked well overall, despite difficulty tracking targets when viewing the unmarked side of the divot. While the results were not optimal, the photogrammetry techniques used for this analysis provided satisfactory results in support of an aggressive flight test and analysis schedule.

Dryden Flight Research Center
National Aeronautics and Space Administration
Edwards, California, March 31, 2006

REFERENCES

1. Corda, Stephen, et al., *The F-15B Lifting Insulating Foam Trajectory (LIFT) Flight Test*, NASA/TM-2006-213674, February 2006.

2. Mikhail, Edward M., James S. Bethel, and J. Chris McGlone, *Introduction to Modern Photogrammetry*, New York, John Wiley & Sons, Inc., 2001.

3. Schairer, Edward T. and Lawrence A. Hand, "Measurements of Unsteady Aeroelastic Model Deformation by Stereo Photogrammetry," AIAA-1997-2217, *Applied Aerodynamics Conference*, Atlanta, GA, June 1997.

4. Plath, W. H., et al., "F/A-18E/F Weapons Separation Wind Tunnel To Flight Test Trajectory and Clearance Comparisons," AIAA 99-0396, the *37th Aerospace Sciences Meeting & Exhibit*, Reno, NV, Jan. 1999.

5. Richwine, David M., *F-15B/Flight Test Fixture II: A Test Bed for Flight Research*, NASA TM-4782, 1996.

6. Yuan, Joseph, "A General Photogrammetric Method for Determining Object Position and Orientation," *IEEE Transactions on Robotics and Automation*, Vol. 5, No. 2, pp. 129-142, 1989.

7. Chen, Fang-Jenq, "Application of Least-Squares Adjustment Technique to Geometric Camera Calibration and Photogrammetric Flow Visualization," *Proceedings of the ISA 43rd International Instrumentation Symposium*, May 1997.

8. Morelli, Eugene A., Stephen D. Derry, Mark S. Smith, "Aerodynamic Parameter Estimation for the X-43A (Hyper-X) from Flight Data," AIAA 2005-5921, *AIAA Atmospheric Flight Mechanics Conference and Exhibit*, Aug. 2005.

9. Bouguet, Jean-Yves, *Camera Calibration Toolbox for MATLAB*,® from the Open Source Computer Vision Library, distributed by Intel and freely available online. Found at http://www.vision.caltech.edu/bouguetj/calib_doc/, a Website maintained by Jean-Yves Bouguet, Ph.D., Intel Corporation, Santa Clara, CA.

10. A*dobe After Effects 6.5, User Guide Supplement*, Adobe Systems, Inc., San Jose, CA, 2004.

11. Etkin, Bernard and Lloyd Duff Reid, *Dynamics of Flight: Stability and Control*, Third edition, John Wiley & Sons, Inc., New York, NY, 1996.

FIGURES

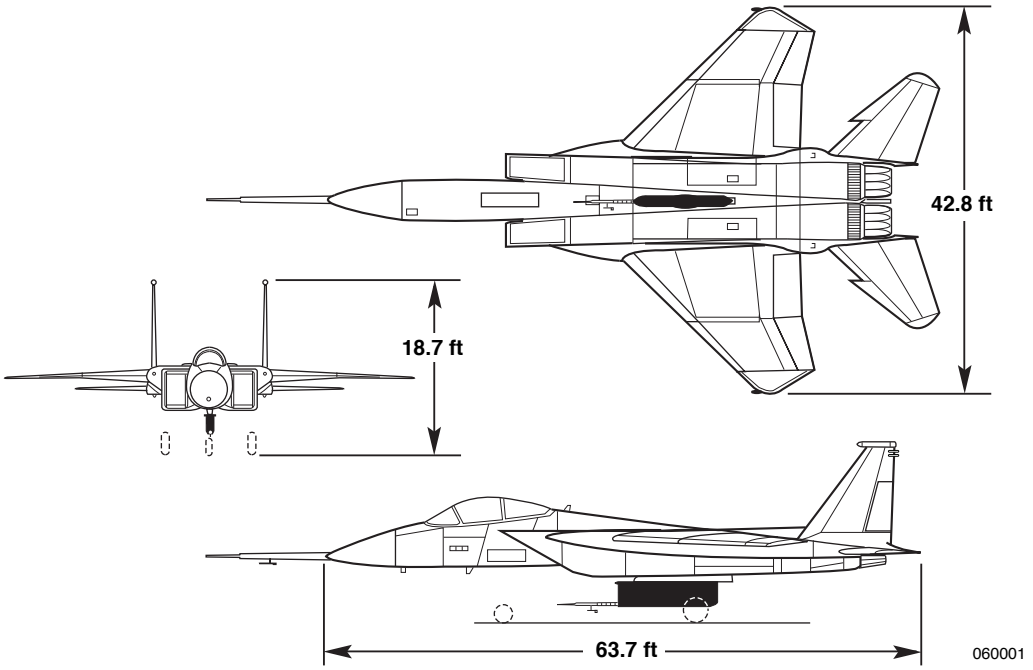

Figure 1. Three-view of test aircraft with AFTF.

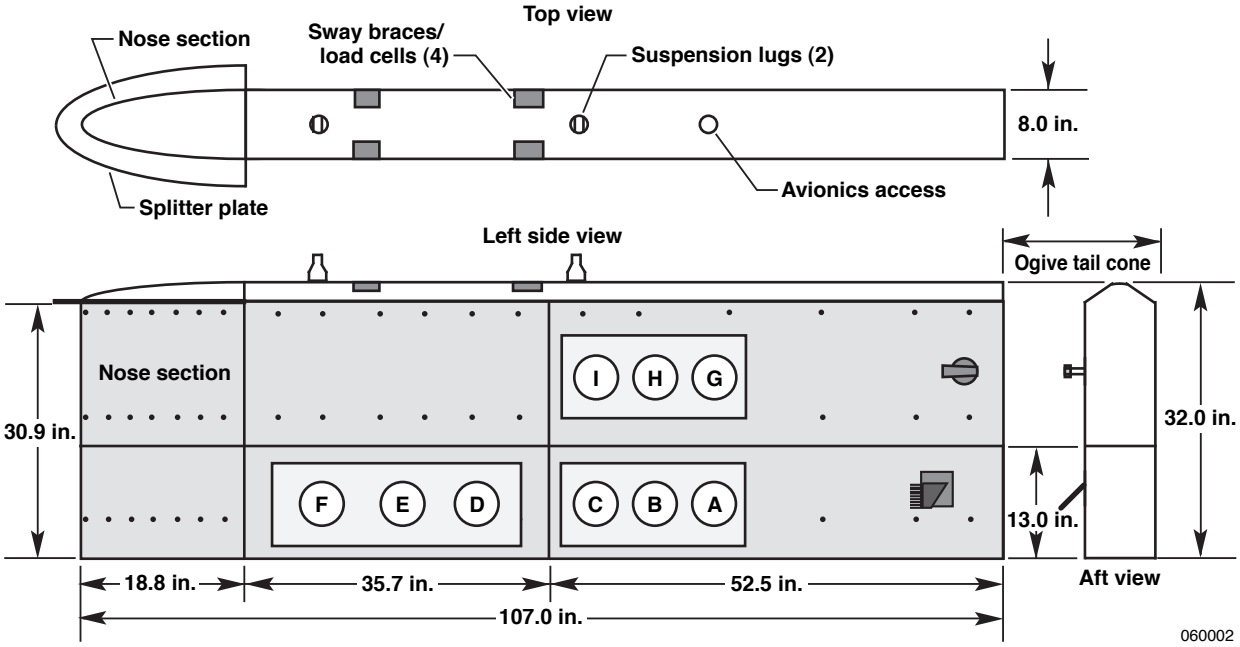

Figure 2. Diagram of AFTF with divot locations (A-G).

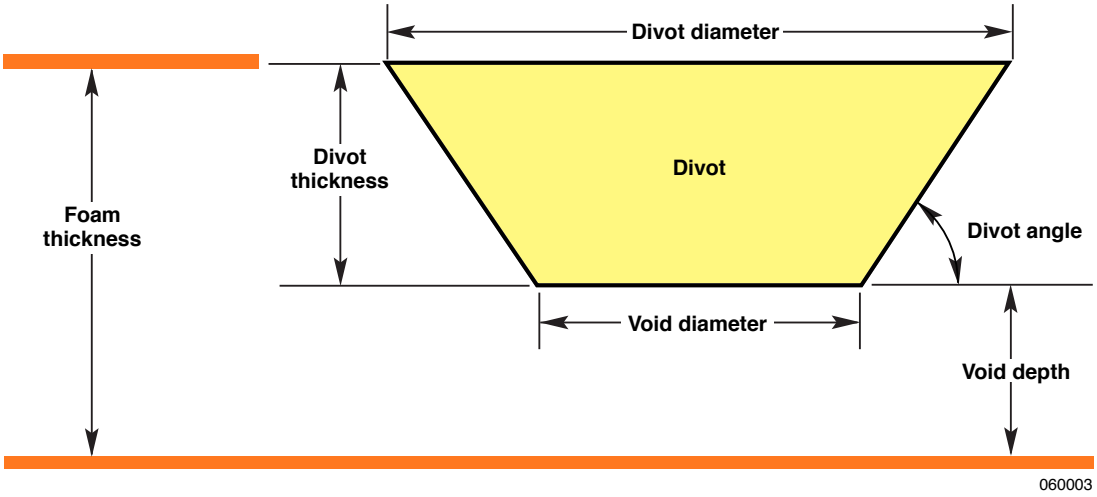

Figure 3. Divot geometry explanation.

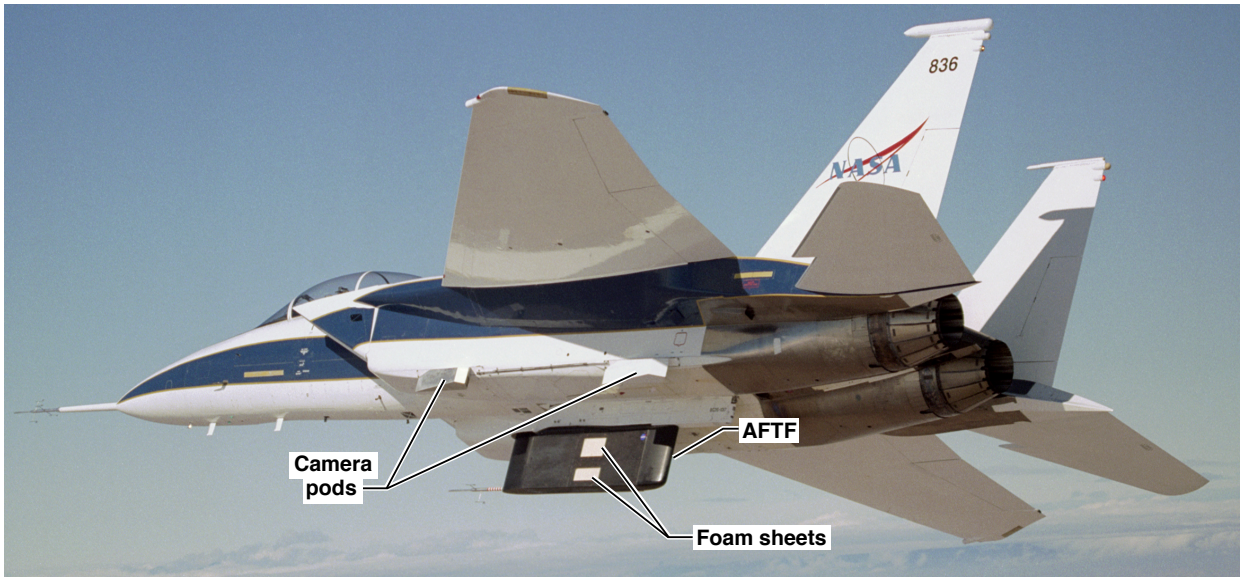

Figure 4. Test aircraft in flight (EC05-0030-12).

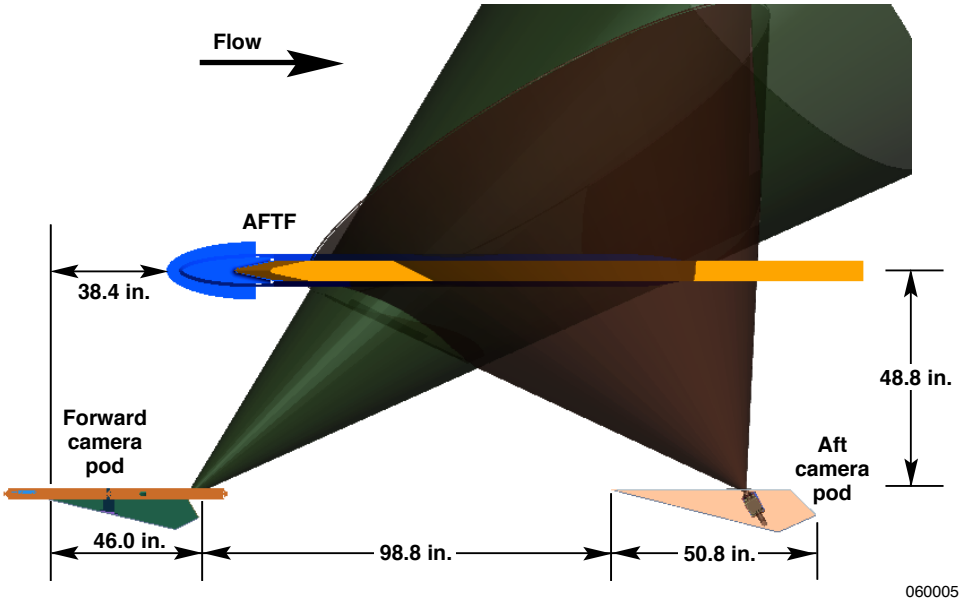

Figure 5. Camera locations and view angles.

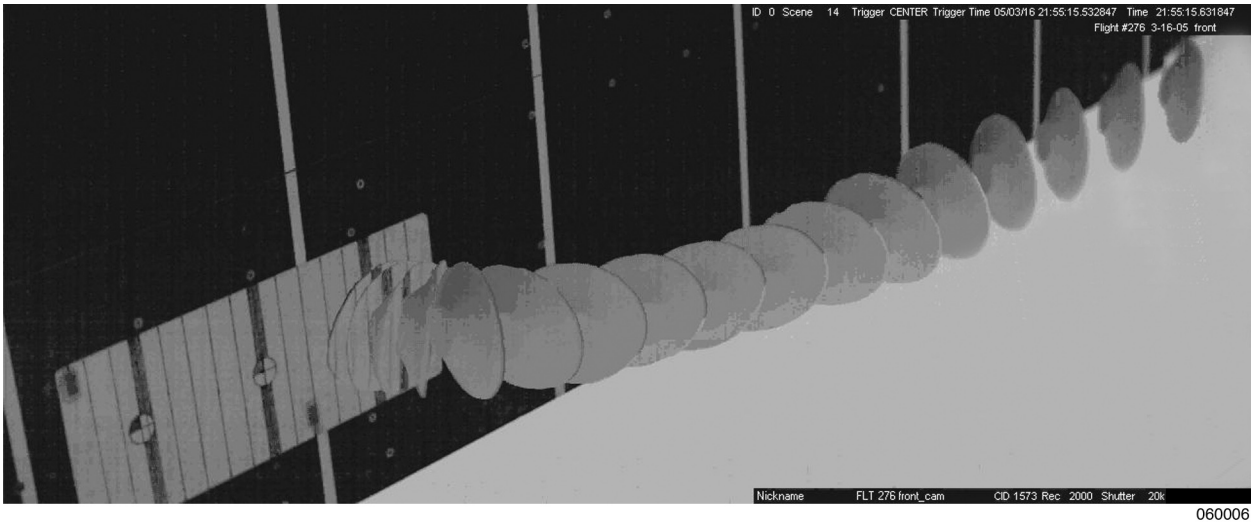

Figure 6. Composite of video frames from divot test (front camera).

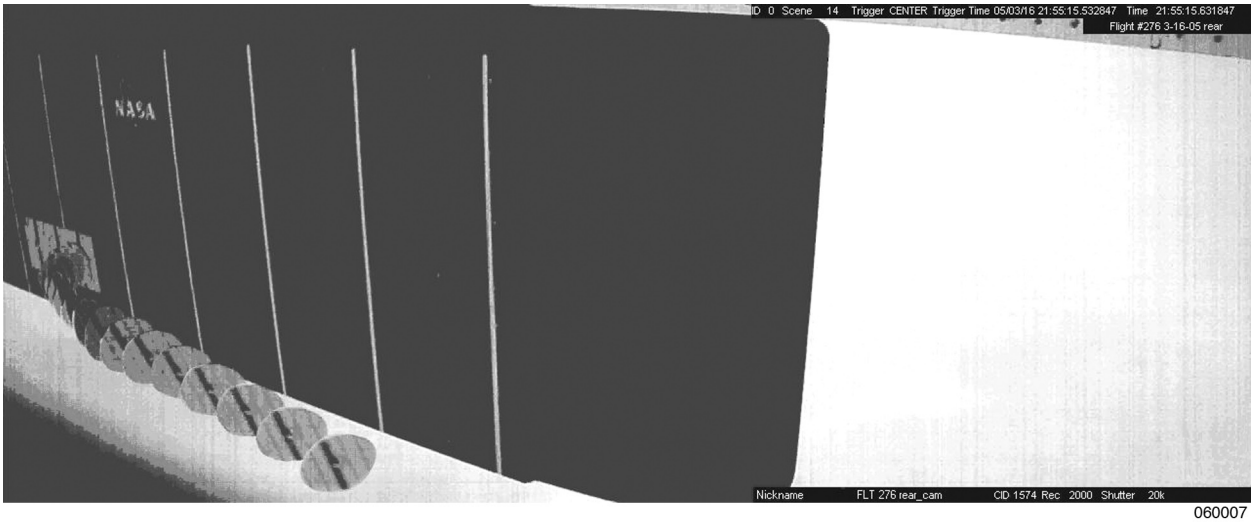

Figure 7. Composite of video frames from divot test (aft camera).

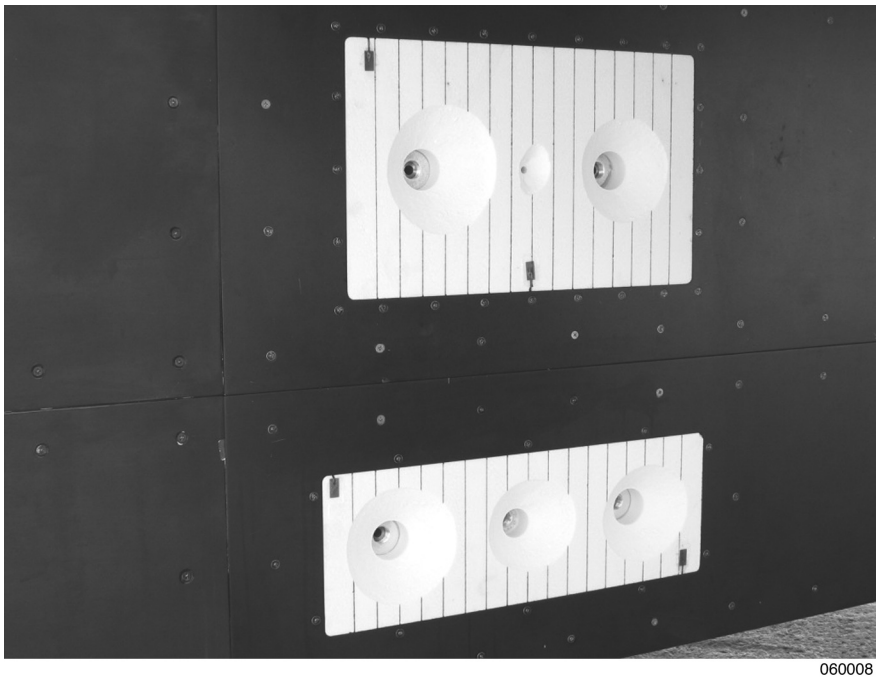

Figure 8. Foam sheets in AFTF post flight.

Figure 9. Calibration fixture as seen from aft camera, with reference axes system.

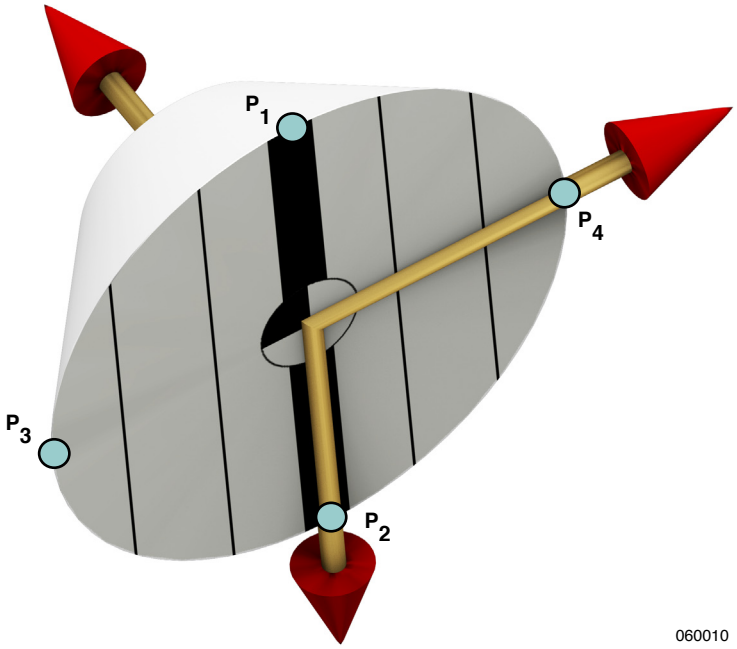

Figure 10. Divot axes system and control point locations.

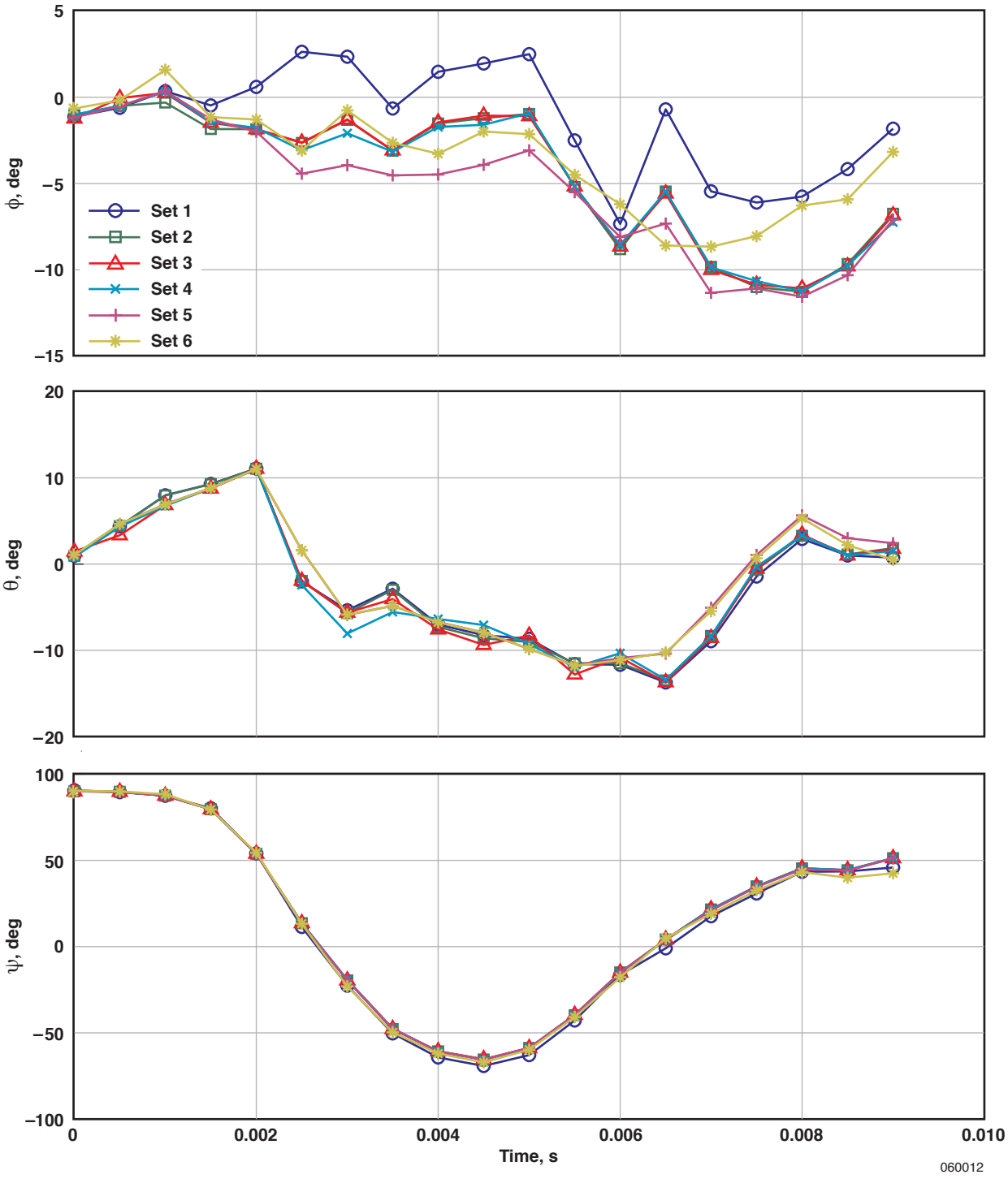

Figure 11. Variation in estimated divot orientation angles due to different sets of control points.

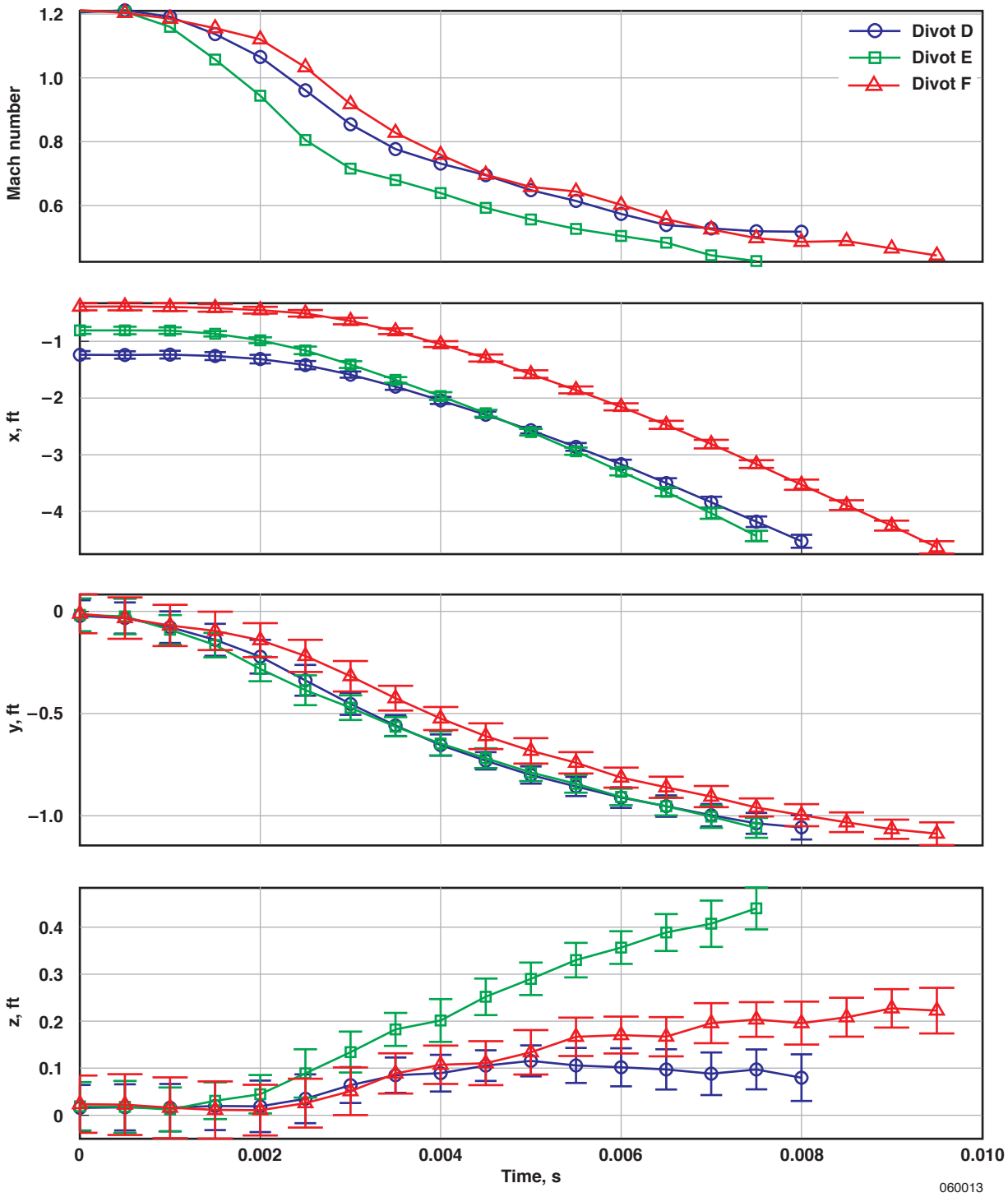

Figure 12. Estimated Mach number and position for Mach 1.2 at 27,000 ft.

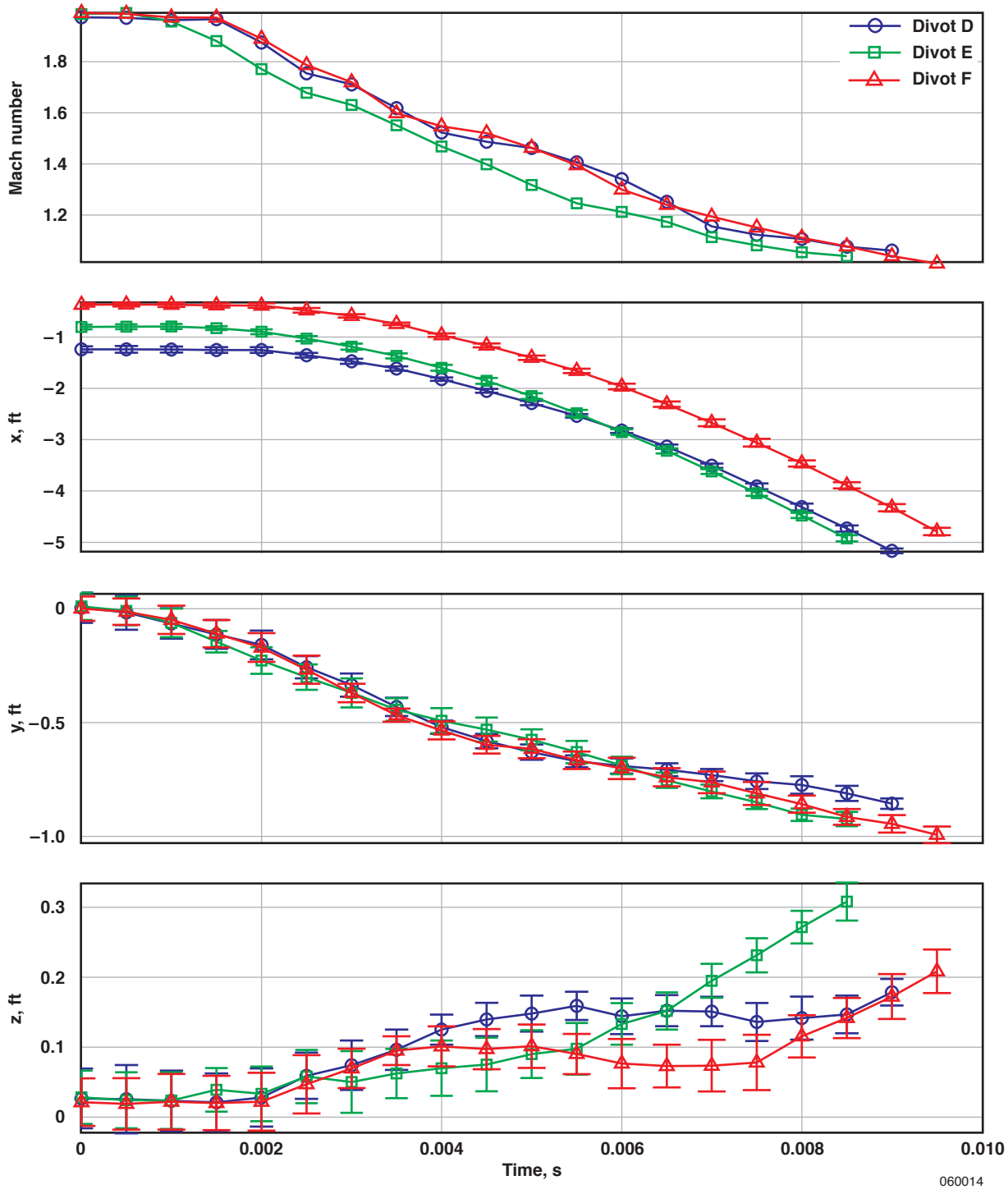

Figure 13. Estimated Mach number and position for Mach 1.98 at 47,000 ft.

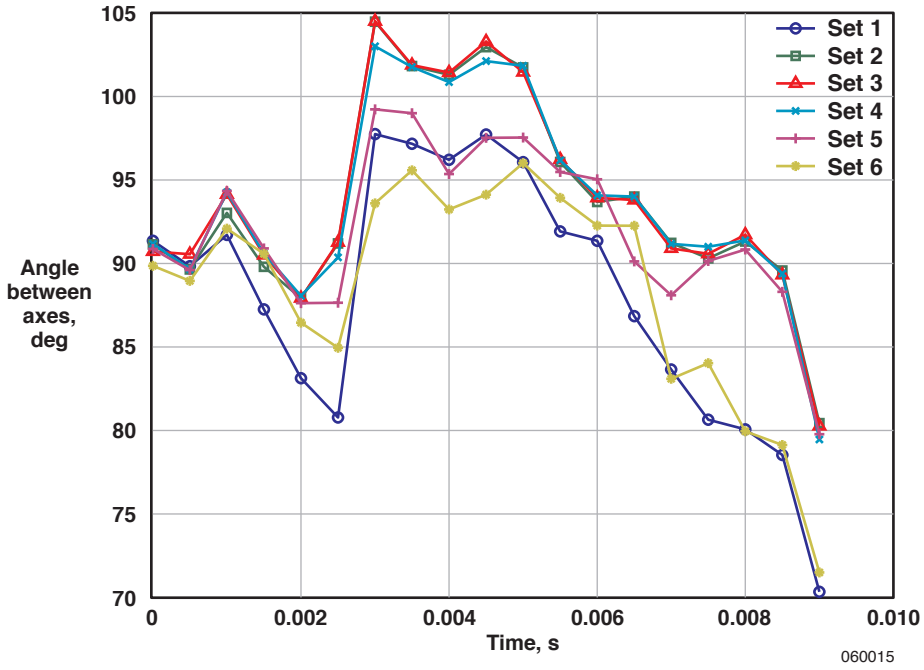

Figure 14. Variation in angle between y- and z-axes for different control points.

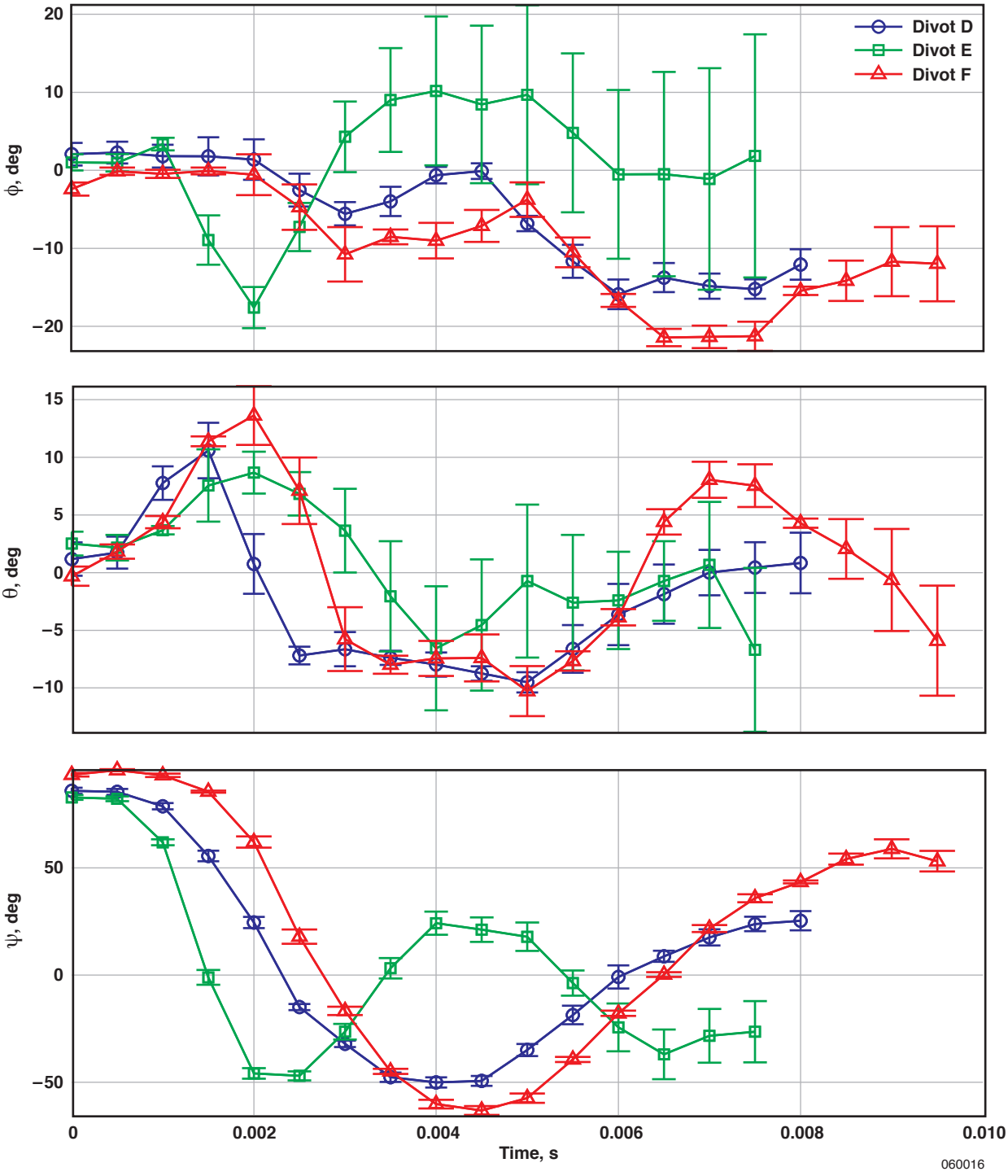

Figure 15. Estimated divot orientations for Mach 1.2 at 27,000 ft.

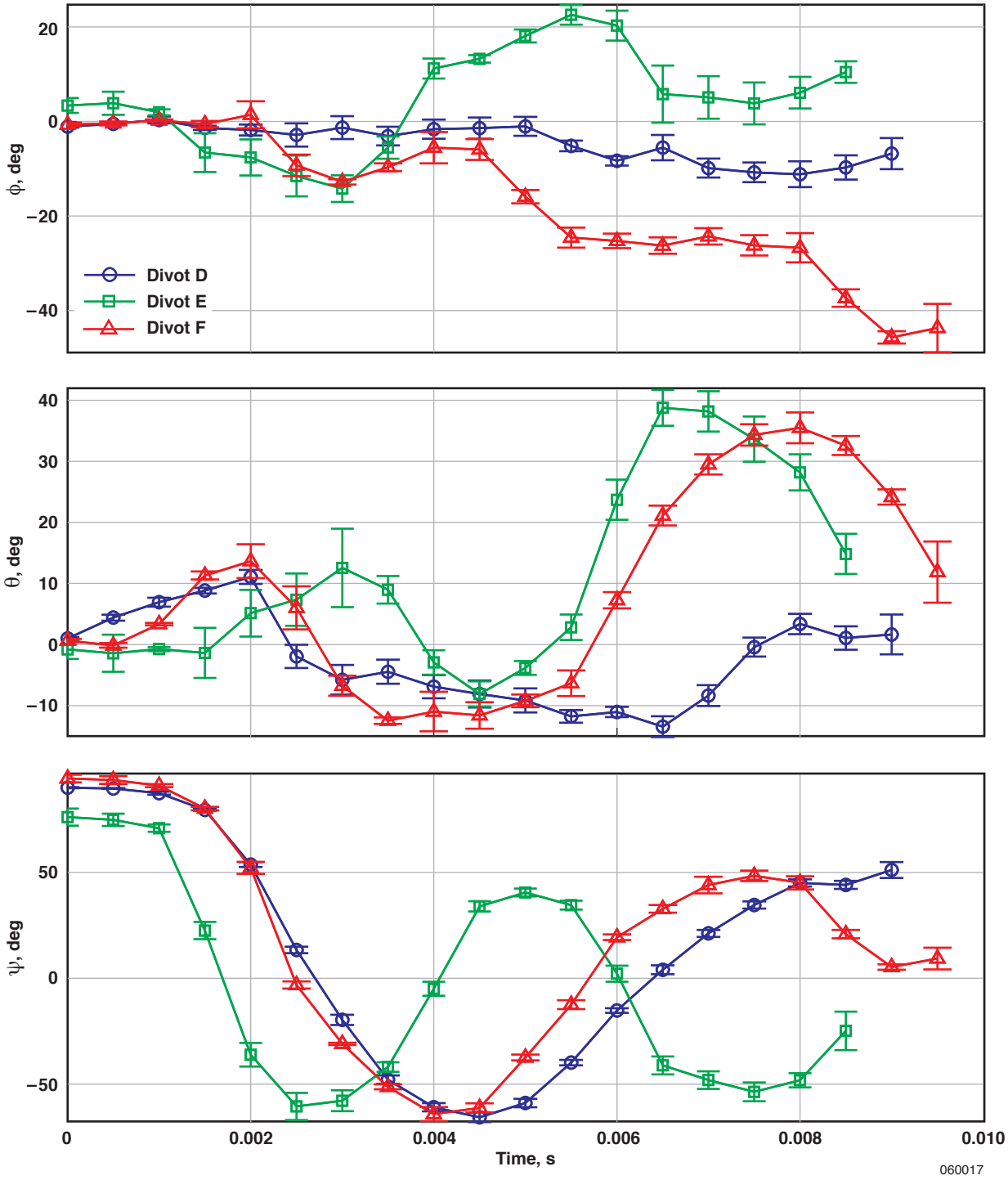

Figure 16. Estimated divot orientations for Mach 1.98 at 47,000 ft.

REPORT DOCUMENTATION PAGE

Form Approved
OMB No. 0704-0188

1. REPORT DATE *(DD-MM-YYYY)*	2. REPORT TYPE	3. DATES COVERED *(From - To)*
28-04-2006	Technical Memorandum	

4. TITLE AND SUBTITLE
Photogrammetric Trajectory Estimation of Foam Debris Ejected From an F-15 Aircraft

5a. CONTRACT NUMBER

5b. GRANT NUMBER

5c. PROGRAM ELEMENT NUMBER

6. AUTHOR(S)
Smith, Mark S.

5d. PROJECT NUMBER

5e. TASK NUMBER

5f. WORK UNIT NUMBER

7. PERFORMING ORGANIZATION NAME(S) AND ADDRESS(ES)
NASA Dryden Flight Research Center
P.O. Box 273
Edwards, California 93523-0273

8. PERFORMING ORGANIZATION REPORT NUMBER
H-2635

9. SPONSORING/MONITORING AGENCY NAME(S) AND ADDRESS(ES)
National Aeronautics and Space Administration
Washington, DC 20546-0001

10. SPONSORING/MONITOR'S ACRONYM(S)
NASA

11. SPONSORING/MONITORING REPORT NUMBER
NASA/TM-2006-213675

12. DISTRIBUTION/AVAILABILITY STATEMENT
Unclassified -- Unlimited
Subject Category 01
Availability: NASA CASI (301) 621-0390
Distribution: Standard

13. SUPPLEMENTARY NOTES

14. ABSTRACT

Photogrammetric analysis of high-speed digital video data was performed to estimate trajectories of foam debris ejected from an F-15B aircraft. This work was part of a flight test effort to study the transport properties of insulating foam shed by the Space Shuttle external tank during ascent. The conical frustum-shaped pieces of debris, called "divots," were ejected from a flight test fixture mounted underneath the F-15B aircraft. Two onboard cameras gathered digital video data at two thousand frames per second. Time histories of divot positions were determined from the videos post flight using standard photogrammetry techniques. Divot velocities were estimated by differentiating these positions with respect to time. Time histories of divot rotations were estimated using four points on the divot face. Estimated divot position, rotation, and Mach number for selected cases are presented. Uncertainty in the results is discussed.

15. SUBJECT TERMS
Camera calibration, Debris, F-15 aircraft, High-speed camera, Photogrammetry

16. SECURITY CLASSIFICATION OF:			17. LIMITATION OF ABSTRACT	18. NUMBER OF PAGES	19a. NAME OF RESPONSIBLE PERSON
a. REPORT	b. ABSTRACT	c. THIS PAGE			STI Help Desk (email: help@sti.nasa.gov)
					19b. TELEPHONE NUMBER *(Include area code)*
U	U	U	UU	29	(301) 621-0390